THE ASTROPHYSICAL JOURNAL, 346:588–600, 1989 November 15

IS THERE STRUCTURE ON THE SCALE OF $300h^{-1}$ Mpc?

MARC POSTMAN
Princeton University Observatory
DAVID N. SPERGEL[1]
Princeton University Observatory
BRIAN SUTIN
University of Maryland
AND
ROMAN JUSZKIEWICZ[2]
Joseph Henry Laboratories, Princeton University; and Institute for Advanced Study, Princeton
Received 1989 February 23; accepted 1989 May 23

ABSTRACT

We explore the existence of very large scale structure in the Abell catalog. Using percolation analysis techniques, we compare the properties of the Tully sample of Abell clusters with simulated cluster catalogs. The simulated catalogs are generated with random distributions and with two-point correlation functions of various amplitudes. The "supercluster complexes" suggested by Tully are not statistically different from clumps generated in simulations with correlation lengths greater than $\sim 15h^{-1}$ Mpc. Our 95% confidence limits on the cluster-cluster correlation length for the Tully sample are $16h^{-1}$ Mpc $\leq R_0 \leq 31h^{-1}$ Mpc. The "flattened" southern Abell cluster distribution is reproduced in the clustered simulations about 20%–30% of the time. This frequency is a function of the correlation length—the Poisson simulations produce such anisotropic distributions only about 6% of the time. The frequency of flattening is independent of the large-scale power cutoff when the cutoff is greater than $\sim 40h^{-1}$ Mpc. Tully's reported structures are real in the sense that they contradict the hypothesis that Abell clusters are randomly distributed. It is likely that the observed effect is due to the superposition of a few superclusters. The present data, however, do not require clustering scenarios which have correlations beyond $\sim 45h^{-1}$ Mpc. If supercluster complexes trace the large-scale distribution of mass and are formed by gravitational instabilities of small initial random phase inhomogeneities, then the predicted perturbations of the cosmic microwave background are in conflict with the current observational limits; in high-density cosmological models, such complexes generate excessive bulk flows. We conclude that there is no definitive evidence for structure on the scale of $300h^{-1}$ Mpc.

Subject headings: cosmology — galaxies: clustering

I. INTRODUCTION

In a recent article, Tully (1987, hereafter T87) suggests the existence for very large scale structure in the Abell catalog (Abell 1958). He claims that the Local Supercluster is only part of a larger structure that he calls a supercluster complex containing $\sim 10^{18} M_{\odot}$. This structure is not only unanticipated in any galaxy formation scenario, but would contradict several "popular" schemes.

The potential importance of this result has prompted us to carefully check its statistical significance. We compare the structures seen in the Abell catalog to structures seen in two sets of simulated catalogs with the same selection effects. In the first set, the simulated clusters are randomly distributed. In the second set, the simulated clusters are laid down with correlation lengths in the range $10h^{-1} \lesssim R_0 \lesssim 30h^{-1}$ Mpc, a range consistent with recent estimates (Bahcall and Soneira 1983; Klypin and Kopolov 1983; Shectman 1985; Postman, Geller, and Huchra 1986; Sutherland 1988; Huchra *et al.* 1989). As usual, the correlation length is defined as the separation at which the two-point correlation function has a value of unity [i.e., $\xi(R_0) = 1$]), Using percolation, we identify large structures in both catalogs and compare their properties. Our objective is to determine how often the structures seen in the Abell catalog are produced in the simulations. We will attempt to contradict two null hypotheses: (1) *Abell clusters are randomly distributed* and (2) *the distribution of Abell clusters is statistically described solely by a two-point correlation function.*

A description of the cluster catalogs used in this analysis is given in § II. The details of the catalog simulation algorithms and a description of the sample selection biases are provided in § III. Analysis of the properties of cluster groups detected by percolation in the real and simulated catalogs and the effects of selection biases on the results are described in § IV. Analysis of the statistical significance and nature of the flattening in the supergalactic plane is discussed in § V. In § VI we present estimates of the large-scale peculiar velocities and perturbations of the cosmic microwave background radiation induced by the existence of massive supercluster complexes. Our conclusions are given in § VII.

II. THE REAL DATA

We use two cluster samples in our analysis. The first is Tully's catalog of 315 Abell clusters (T87) with measured redshifts $z \leq 0.1$ and richness class $R \geq 0$. Of the 315 clusters, 201 are in the north Galactic hemisphere and 114 are in the south Galactic hemisphere. Tully estimates that the sample is 100%

[1] Alfred P. Sloan Fellow; NSF Presidential Young Investigator.
[2] On leave from Warsaw University Observatory and Copernicus Center, Warsaw, Poland.

complete to $z = 0.06$, 70% complete to $z = 0.075$, and 50% complete to $z = 0.1$. There are no angular position limits other than the $\delta = -27°$ cutoff of the Abell catalog.

The second catalog consists of all Abell clusters with $m_{10} \leq 16.4$. There are 277 clusters in this sample, all of which now have measured redshifts (Huchra, Geller, and Postman 1989). Of the 277 clusters, 176 are in the north Galactic hemisphere and 101 are in the south Galactic hemisphere. The maximum cluster redshift in this sample is 0.1470; however, 92% of the cluster redshifts are less than 0.1. We shall hereafter refer to this catalog as the whole sky sample. The completeness of the whole sky sample is comparable with that of the Tully sample as there is substantial overlap between the two catalogs (the samples have 231 clusters in common). We will use the whole sky sample to verify the large-scale flattening reported in T87 and to provide one estimate of the redshift selection function for $z \leq 0.1$ Abell clusters.

About 90% of the clusters in both samples lie at least 25° above (or below) the Galactic plane. Figures 1 and 2 show projections of the two samples as viewed along the axes of the supergalactic coordinate system. Distance units are h^{-1} Mpc. Comoving distances to clusters are computed from redshifts using standard Friedmann cosmology (Mattig 1958):

$$R = \frac{c}{H_0 q_0^2(1+z)} [q_0 z + (q_0 - 1)(\sqrt{2q_0 z + 1} - 1)] . \quad (1)$$

We use $H_0 = 100$ km s^{-1} Mpc^{-1} and $q_0 = 0.1$. Here $q_0 = \Omega_0/2$ is the usual deceleration parameter, and we assume zero cosmological constant.

III. CLUSTER CATALOG SIMULATIONS

a) Simulation Algorithms

We generate three sets of catalogs. In the first set of catalogs, the points corresponding to Abell clusters are randomly placed in the simulation. In the second set of catalogs, the underlying cluster distribution is completely described statistically by the two-point correlation function. In the third set of catalogs, the underlying cluster distribution corresponds to the peaks of a Gaussian random field.

In each set of simulations, points are placed into a $640h^{-1} \times 640h^{-1} \times 640h^{-1}$ Mpc cube. Points outside of a $640h^{-1}$ Mpc diameter sphere are rejected. We then impose both redshift and angular selection: rejecting first a fraction

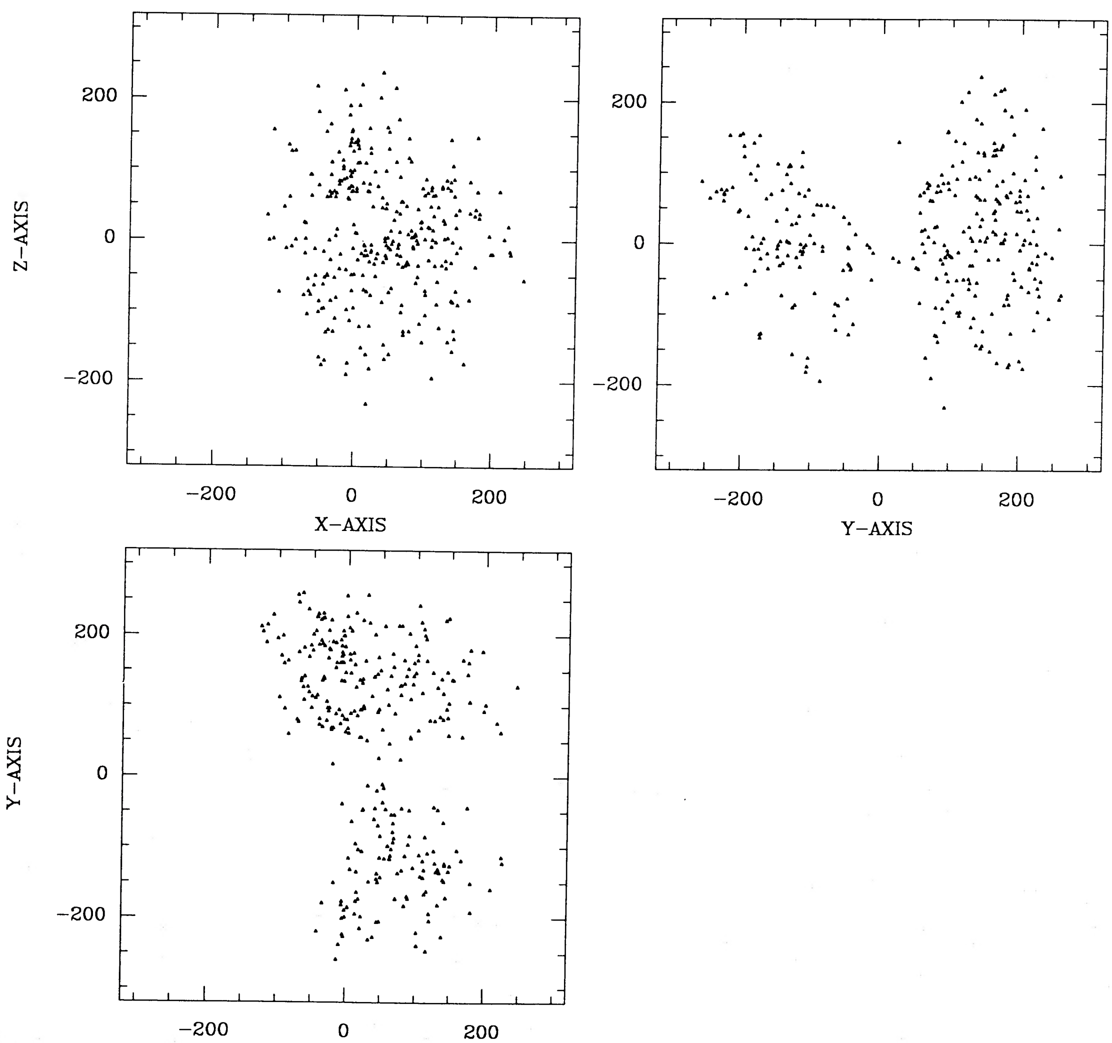

FIG. 1.—Projections of the cluster distribution in supergalactic coordinates for the Tully sample. Plane of the galaxy lies nearly parallel to the supergalactic X-Z plane.

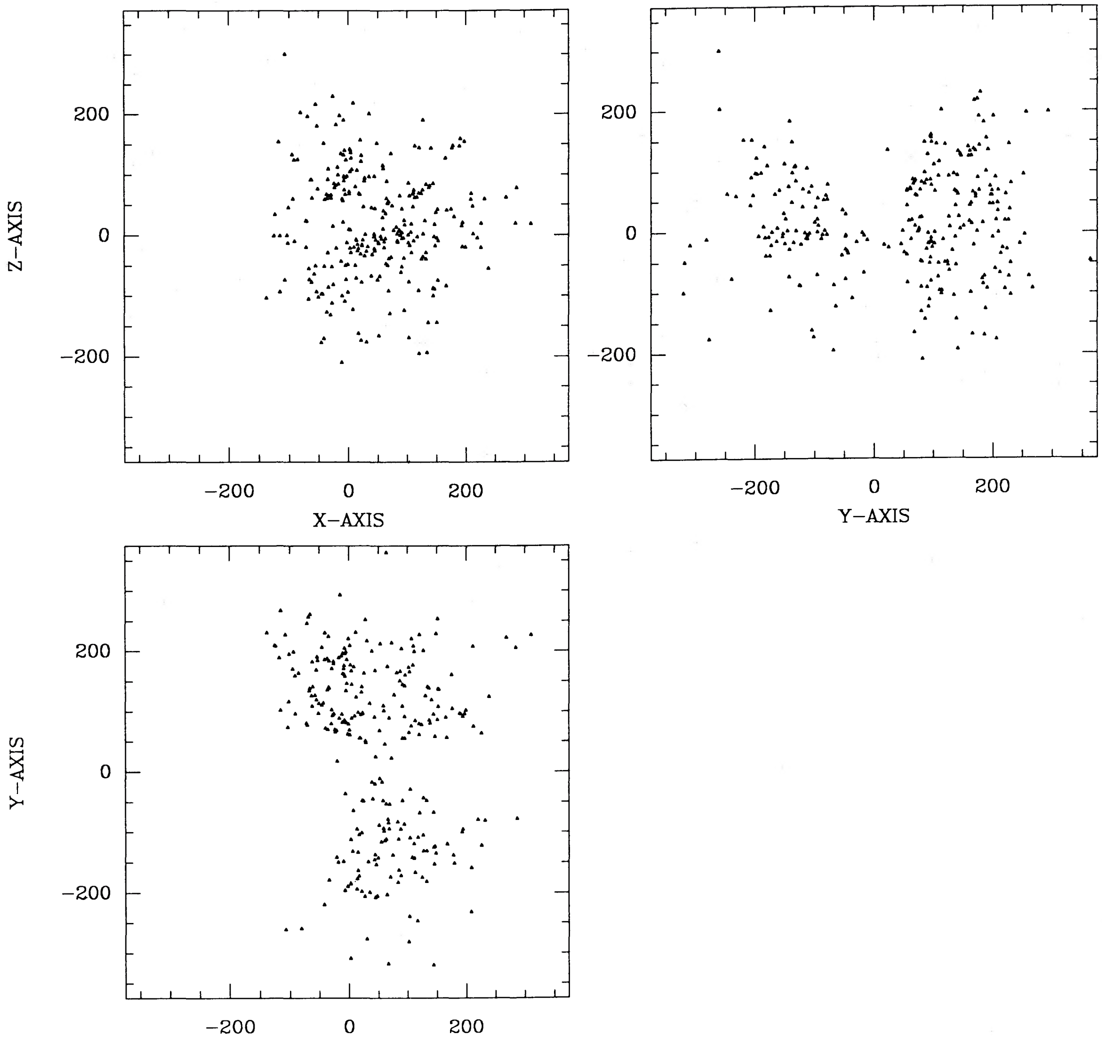

FIG. 2.—Projections of the cluster distribution in supergalactic coordinates for the whole sky sample

$f_1(z)$ of points and then rejecting a fraction $f_2(l, b)$ of the remaining points. Section III*b* describes the selection functions applied to the data. In all the simulations the number of clusters in the north and south Galactic hemispheres is the same as in the real Tully sample.

The clusters in the second set of simulations have two-point correlations generated from a velocity field. This velocity field is produced in 2^{18} $10 \times 10 \times 10h^{-3}$ Mpc^3 boxes. The clusters are randomly placed within a box and assigned a velocity using the cloud-in-cell (CIC) algorithm (Efstathiou *et al.* 1985), which assures a continuous velocity field. The clusters are then displaced by Δx, which is proportional to the velocity field at that point. The density field in k-space is converted to a velocity field by multiplying the value of the k-space density contrast at each grid point by $i\boldsymbol{k}/|\boldsymbol{k}|^2$. Taking the Fourier transform then gives the three spatial components of the peculiar velocity at each point in the grid. The density fluctuations have a power spectrum with real and imaginary components Gaussian-distributed about zero with dispersion

$$P(|\boldsymbol{k}|) = w|\boldsymbol{k}|^n \exp\left(\frac{-|\boldsymbol{k}|^2}{\Lambda^2}\right)\Theta(|\boldsymbol{k}|) , \qquad (2)$$

where w, a normalization factor, and n, the slope of the power spectrum, can be adjusted to give simulations with different correlation functions. The exponential term cuts off the power spectrum at large k corresponding to small spatial scales. We use $\Lambda = 10h$ Mpc^{-1} in agreement with the observed cluster-cluster correlation function (Bahcall and Soneira 1983; Huchra *et al.* 1989). The step function $\Theta(|\boldsymbol{k}|)$ is used to cut off the power spectrum at small k corresponding to large spatial scales. This technique, the Zel'dovich approximation applied to Gaussian random initial conditions, is used to generate initial conditions in N-body simulations (Efstathiou *et al.* 1985). As long as the cluster-cluster correlation length is less than $17h^{-1}$ Mpc, this technique reproduces the two-point correlation function with the observed form. For larger correlation length, the Zel'dovich approximation breaks down, and we are no longer able to reproduce a power-law correlation function.

In the third set of simulations, clusters are assigned to peaks of a Gaussian random field. Kaiser (1984*b*) suggested that Nature used this algorithm in forming Abell clusters and that this accounts for the large amplitude of the cluster-cluster correlation function. In this simulation, the underlying density field is the Fourier transform of a Gaussian random field with the power spectrum given in equation (2). Clusters are randomly assigned to boxes in which the amplitude of the density contrast exceeds a minimum threshold. Using this algorithm, we generate samples with high-amplitude two-point correlation functions. Since the distribution of peaks of a Gaussian field is non-Gaussian, the clusters in this simulation have nonzero higher order correlations.

The normalization and slope of the power spectrum are adjusted to produce simulations with correlation lengths in the range $10h^{-1}$ Mpc $\leq R_0 \leq 30h^{-1}$ Mpc and correlation function slopes in the range $-1.7 \leq \gamma \leq -1.9$. The values of the power spectrum parameters which yield the desired correlation functions are $w = 0.6$ and $-0.7 \leq n \leq -0.5$ for the Zel'dovich CIC simulations and $w = 1.0$ and $-0.9 \leq n \leq -0.6$ for the Gaussian peak simulations. The minimum density threshold used in the Gaussian peak simulations corresponds to 1.5 σ fluctuations. Unless otherwise specified all clustered simulations with correlation lengths greater than $17h^{-1}$ Mpc are generated with the Gaussian peak algorithm and all clustered simulations with smaller correlation lengths are generated with the Zel'dovich CIC algorithm.

b) Selection Biases

Selection biases in redshift and Galactic latitude dominate the incompleteness in the real cluster catalogs used in this study. In order to measure the importance of these biases on our results we introduce similar selection effects in the simulations. Two empirical estimates for the redshift selection function are used. The first, hereafter referred to as the full redshift selection function, is derived from the redshift distribution of all high Galactic latitude ($|b| \geq 30°$) $R \geq 0$ Abell clusters with measured redshifts. There are currently 628 high-altitude Abell clusters (out of a possible 2473) with measured redshifts. The second, hereafter referred to as the magnitude-limited redshift selection function, is derived from the redshift distribution of the 231 high-latitude clusters in the whole sky sample described in § II. The redshift selection function is just the probability that a cluster in the range z to $z + \Delta z$ would have been included in the Abell catalog. It is estimated by taking the ratio of the number of observed clusters in the range z to $z + \Delta z$ to the number of clusters expected in a uniform dis-

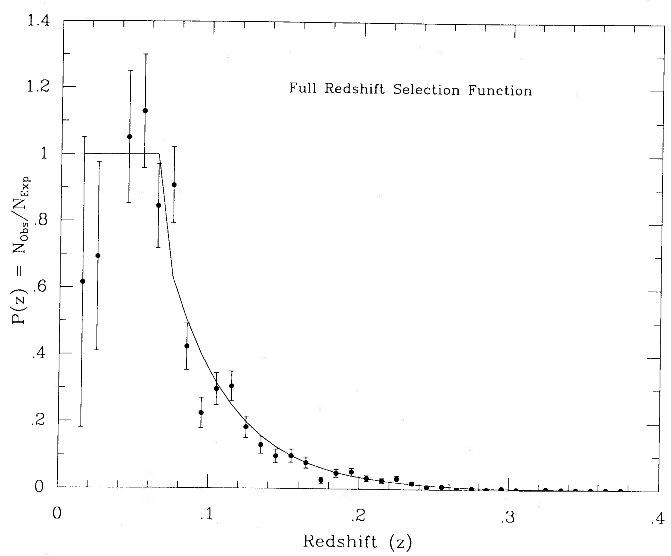

FIG. 3*a*

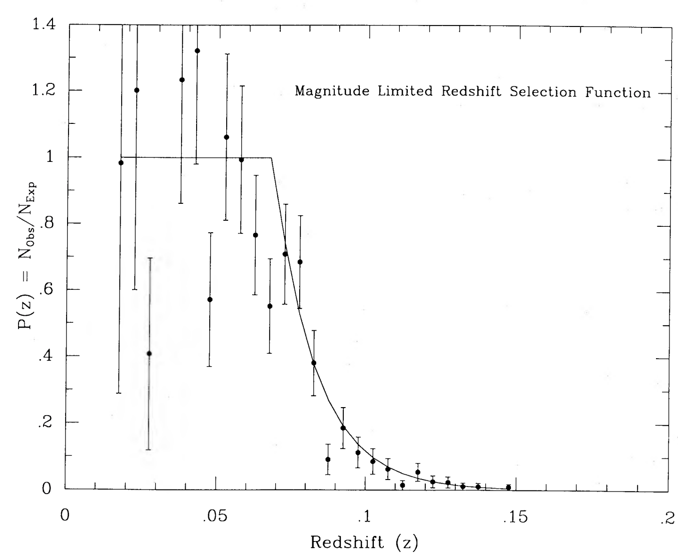

FIG. 3*b*

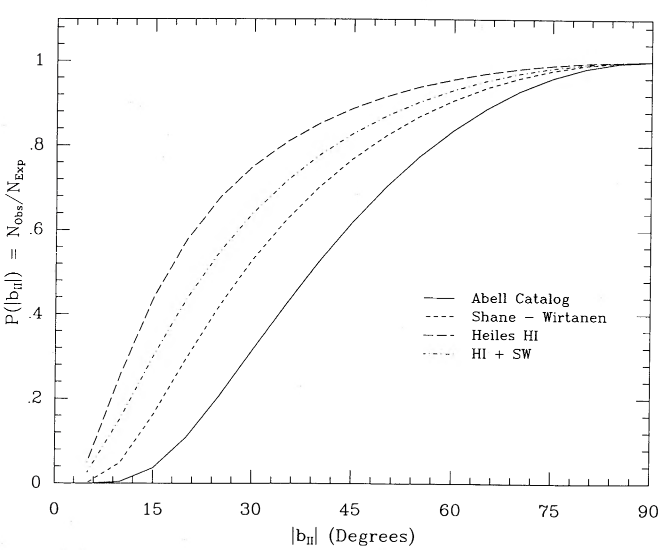

FIG. 3*c*

FIG. 3.—(*a*) Selection probability as a function of redshift for all high Galactic latitude ($|b| \geq 30°$) $R \geq 0$ Abell clusters with measured redshifts. Error bars show $N^{1/2}$ uncertainties. The best fit for $z > 0.07$ is $P(z) = 3.6365 \exp(-z/0.0429)$. (*b*) Selection probability as a function of redshift for the high Galactic latitude ($|b| \geq 30°$) $R \geq 0$ Abell clusters in the whole sky magnitude-limited sample. The best fit for $z > 0.07$ is $P(z) = 101.1219 \exp(-z/0.0148)$. (*c*) Selection probability as a function of Galactic latitude as derived from the Abell catalog, Shane-Wirtanen (SW) catalog, and the Heiles H I survey. The Abell and SW selection functions are the best-fit cosecant extinction laws. The H I selection function is derived from data in Burstein and Heiles (1978) and Fisher and Tully (1981).

tribution. Figure 3*a* and 3*b* show the redshift selection function for the full and magnitude-limited cluster samples, respectively. The fits shown are of the form

$$P(z) = 1 \quad \text{for} \quad z \leq z_c \tag{3a}$$

$$P(z) \propto \exp(-z/z_0) \quad \text{for} \quad z > z_c \,, \tag{3b}$$

where z_c is the maximum redshift at which the sample is 100% complete and z_0 is a scaling constant. Both selection functions indicate ~100% completeness out to $z = 0.07$, in agreement with Tully's estimate. All of our simulations are redshift-limited at $z = 0.1$ to match the Tully cluster sample. Simulations generated with the full redshift selection function will therefore have a relatively higher fraction of clusters in the range $0.07 < z \leq 0.1$ than simulations generated with the magnitude-limited redshift selection function.

We compute estimates of the Galactic latitude selection function from three different sources: the Abell catalog, the Shane-Wirtanen (hereafter SW) galaxy catalog (Shane and Wirtanen 1967), and the Heiles H I survey (Heiles 1975). The selection functions derived from the Abell and Shane-Wirtanen catalogs are determined directly from number counts as a function of Galactic latitude. Consequently, it is possible that the Abell or SW selection functions may be biased by the presence of a large-scale feature near the Galactic pole. To minimize this potential bias, the Abell latitude selection function is based on the entire catalog—any nearby structure should thus be washed out by superpositions. The SW selection function is taken from Burstein and Heiles (1978). The selection function derived from the H I survey (Burstein and Heiles 1978; Fisher and Tully 1981), which is a function of both Galactic latitude and longitude, is not biased by the presence of any extragalactic structure. Figure 3*c* shows the best fits to the Galactic latitude selection functions for the Abell catalog, SW catalog, and H I survey. The H I selection function shown is an average over all Galactic longitudes. In the Monte Carlo simulations generated with the H I selection function, the longitude dependence is included. Also shown in Figure 3*c* is an average of the H I and SW selection functions (hereafter H I+SW). All the latitude selection functions in Figure 3*c* are consistent with a cosecant extinction law of the form

$$P(|b|) = \text{dex}\,\{\alpha[1 - \beta \csc(|b_{\rm II}|)]\} \,. \tag{3c}$$

For reference, the SW selection function is in excellent agreement with the latitude selection function derived by Bahcall and Soneira (1983) for the 104 clusters in their $D \leq 4$ sample ($\alpha \approx 0.3$, $\beta \approx 1.0$).

IV. PERCOLATION AND PRINCIPAL COMPONENT ANALYSIS

We now compare the properties of groups detected by percolation in the Tully cluster catalog with those in the simulated catalogs as a function of the percolation length, the correlation length, and the selection biases. For this analysis we use Poisson simulations and simulations with correlation lengths of 12, 14, 17, 20, and $24h^{-1}$ Mpc and correlation function slope = −1.8 (±0.1). The power spectra of all the clustered simulations are cut off at small wavenumbers corresponding to spatial separations greater than $80h^{-1}$ Mpc. Our percolation algorithm works in the usual way—centering on a given cluster and assigning group membership to all clusters which are within a specified distance (the percolation length) from the central cluster. All the group members are then searched for "friends" until no new members are found. Groups are required to contain a minimum of five members. The group morphology and volume are estimated using principal component analysis (as in T87): each system is represented by a triaxial spheroid with dimensions computed from the rms deviations about the center of mass. We analyze the north and south Galactic hemispheres separately to avoid cluster linkages across the Galactic plane. Table 1 lists some properties of the cluster complexes in the Tully sample as a function of the percolation length. The percolation length is listed in column (1). The mean 1 σ volume and the mean total population of the complexes are listed in columns (2) and (3), respectively. Columns (4), (5), and (6) list the mean dimensions of the 1 σ spheroid. The mean number density enhancement of the complexes is listed in column (7), and the total number of complexes found at each percolation length is listed in column (8).

Figure 4*a* shows the fraction of the total available volume occupied by the 1 σ surfaces of the detected groups as a function of the percolation length for the Tully sample and simulations with the indicated correlation lengths. Figure 4*b* shows the fraction of the total number of clusters in groups as a function of the percolation length. The results for the simulations are the average results for 50 realizations. The error bars shown are the 1 σ standard deviations for one set of 50 realizations. Errors for the other simulations are omitted for the sake of clarity but are of comparable magnitude. The simulations were generated using the magnitude-limited redshift selection function and the H I+SW Galactic latitude selection function. The observed trends are as expected—at a given percolation length the fraction of clusters in groups increases with increasing correlation length. The population fraction appears to be more sensitive to the correlation length than the volume fraction. We confirm Tully's claim that at a percolation length of $28h^{-1}$ Mpc, the scale at which the maximum percolation dimension approaches the effective depth of the sample, the 1 σ surfaces of the detected groups in the Tully sample occupy 0.4% of the total volume. The dimensions defined by the 1 σ surfaces are, however, significantly smaller than the sample depth (see Table 1). For comparison, at this same percolation

TABLE 1

MEAN PROPERTIES OF TULLY GROUPS

λ (Mpc) (1)	1 σ Volume (Mpc^3) (2)	Total Population (3)	σ_a (Mpc) (4)	σ_b (Mpc) (5)	σ_c (Mpc) (6)	$\frac{\delta n}{n}$ (7)	$N_{\rm grps}$ (8)
20.....	2.00×10^3	5.8	2.0	5.9	13.1	31.0	5
30.....	4.97×10^4	12.7	7.2	15.6	29.1	6.70	11
40.....	2.02×10^5	19.7	12.2	19.6	38.0	2.03	11
50.....	1.55×10^6	68.3	26.4	33.3	55.4	0.23	4
60.....	3.70×10^6	150.5	49.8	65.6	88.8	0.02	2
70.....	3.92×10^6	156.0	50.8	66.7	90.6	0.01	2

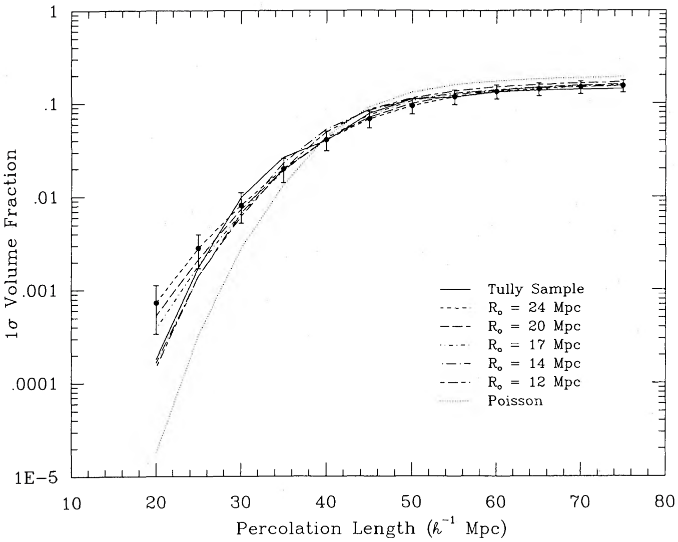

FIG. 4*a*

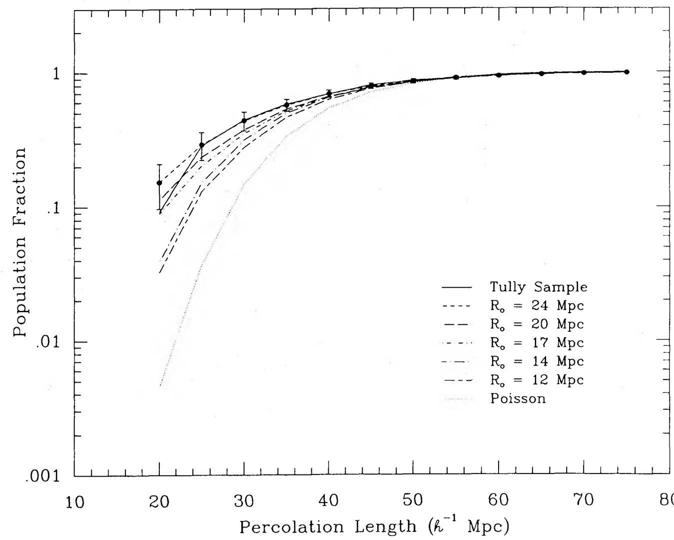

FIG. 4*b*

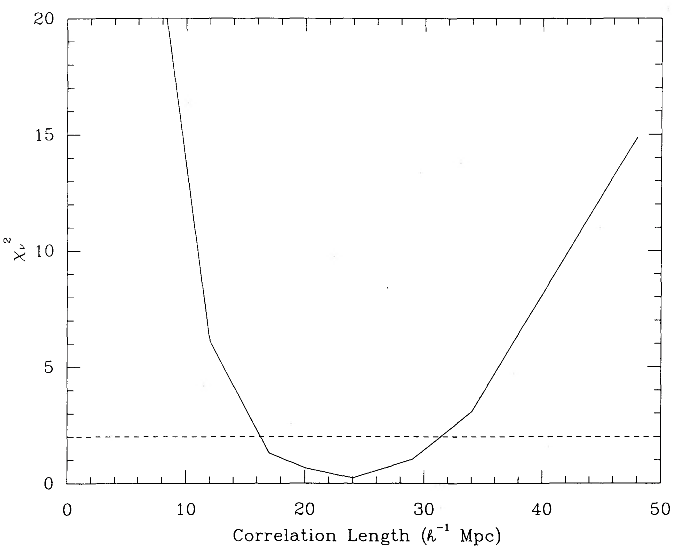

FIG. 4*c*

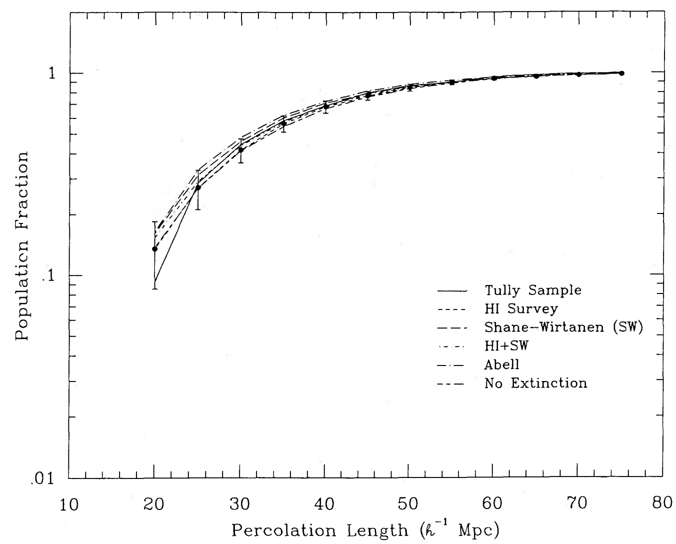

FIG. 4*d*

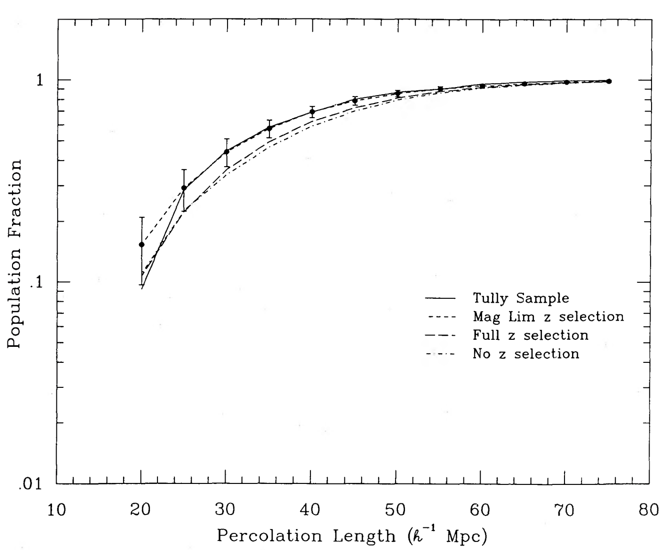

FIG. 4*e*

FIG. 4.—(*a*) One sigma volume filling fraction of the detected supercluster complexes as a function of percolation length for the Tully cluster sample. The mean results for simulations with random and clustered distributions are also shown. The error bars are the 1 σ uncertainties for one of the simulation sets. (*b*) Fraction of the total cluster sample in supercluster complexes as a function of percolation length for the Tully sample and simulations. (*c*) Reduced χ^2 as a function of the correlation length for fits between the observed population fraction–percolation length curve and those for the simulations. Fitting was limited to percolation lengths $\leq 50h^{-1}$ Mpc. The 95% confidence limits (where the reduced χ^2 is less than ~ 2) are $16h^{-1}$ Mpc $\leq R_0 \leq 31h^{-1}$ Mpc. (*d*) Fraction of the total cluster sample in supercluster complexes as a function of the percolation length and the Galactic latitude selection function. Redshift selection function held constant. (*e*) Fraction of the total cluster sample in supercluster complexes as a function of the percolation length and the redshift selection function. Galactic latitude selection function held constant.

length in the simulations with $R_0 = 24h^{-1}$ Mpc, the 1 σ volume fraction is about 0.005 (0.5%). In the simulations with $R_0 = 12h^{-1}$ Mpc the volume fraction at this percolation length is about 0.003 (0.3%). The mean volume fraction in the Poisson simulations is only about 0.001 (0.1%). In general, for percolation lengths less than about $45h^{-1}$ Mpc, the simulations with $R_0 \gtrsim 15h^{-1}$ Mpc yield the best agreement with the data. At larger percolation lengths both the clustered and Poisson simulations yield groups with similar properties as those in the Abell catalog. This is not surprising since the mean separation between clusters in the Tully sample (and in the simulations) is about $42h^{-1}$ Mpc.

The sensitivity of the population fraction to the correlation length for percolation lengths less than $50h^{-1}$ Mpc provides another way of determining acceptable limits on the correlation length of the Tully cluster sample. Figure 4*c* shows the reduced χ^2 value as a function of the correlation length for fits between the observed population fraction–percolation length curve and those for the simulations. Fitting was restricted to percolation lengths $\leq 50h^{-1}$ Mpc. For this particular calculation, we generated three additional clustered simulation sets with correlation lengths of 29, 34, and $48h^{-1}$ Mpc (all with correlation function slope = -1.8). The best-fit correlation length for the Tully sample is $24h^{-1}$ Mpc. The 95% confidence limits are $16h^{-1}$ Mpc $\leq R_0 \leq 31h^{-1}$ Mpc.

We next generate a series of simulations with constant correlation length ($R_0 = 24h^{-1}$ Mpc) but with different selection functions in order to assess their effect on the above results. Figure 4*d* shows the population fraction as a function of the percolation length for five simulation sets with different Galactic latitude selection functions (but all with the same redshift selection function). Again, the results for each simulation set are the mean results for 50 realizations. The 1 σ error bars for one of the simulation sets are also shown. The effect of varying Galactic extinction varies the dependence of population fraction on percolation length at less than the 1 σ level. (The same is true for other group properties such as the volume fraction.) Varying the redshift selection function has a slightly larger effect on the results, as shown in Figure 4*e*, but the shifts are still only at about the 1 σ level. The fact that at a given percolation length there are slightly fewer clusters associated with groups when we use the full redshift selection function or no redshift selection is due to the relatively higher fraction of clusters located near the $z = 0.1$ limit in these simulations. Consequently, the mean cluster separation is slightly higher and the samples tend to percolate at slightly larger lengths. We thus conclude, in agreement with Tully, that selection effects do not strongly affect these results.

The variation of group morphology with percolation length is displayed in Figures 5*a* and 5*b*. Figure 5*a* shows the histograms of group axial ratios for the Tully sample and for the clustered simulation set with $R_0 = 24h^{-1}$ Mpc. Figure 5*b* shows the histograms of group axial ratios for the Tully sample and for a Poisson simulation set. The triangular data points represent the axial ratio histograms of the Abell cluster groups. The solid line histograms are the mean distributions for 50 realizations. The shaded areas represent the 90% confidence limits on the mean distributions. There are naturally many fewer groups found in the Poisson simulations than in the Tully sample at percolation lengths less than $40h^{-1}$ Mpc. The shapes of the "supercluster" complexes in the clustered simulations are consistent with those in the Abell catalog at all percolation lengths. The probability of a very elongated (axial ratio > 10) complex forming in the Poisson simulations is slightly lower than in the clustered simulations probably due to the higher occurrence of chance superpositions in the clustered simulations. However, at percolation lengths greater than $40h^{-1}$ Mpc, there is no significant difference between the group morphologies in the clustered simulations and those in the Poisson simulations.

It is also interesting to determine if the above analysis methods can find any differences between the complexes found in simulations generated using the Zel'dovich CIC algorithm and those found in simulations where clusters are placed at the peaks of a Gaussian random field. We generate two clustered simulation sets with each algorithm, both sets of simulations having the same correlation length, $R_0 = 15h^{-1}$ Mpc, and the same correlation function slope, $\gamma = -1.8$. Each simulation set consists of 50 realizations. We find the two simulation sets have essentially identical properties. No significant differences on small or large scales can be found. The above properties either do not depend strongly on the higher order moments of the cluster distribution and/or percolation and principal component analysis are not very sensitive probes of higher order moments.

V. LARGE-SCALE FLATTENING

The most fundamental claim in T87 is that the nearby ($cz \lesssim$ 23,000 km s^{-1}) Abell clusters in the south Galactic hemisphere preferentially lie in the same plane as that defined by the distribution of nearby ($cz \lesssim 3000$ km s^{-1}) galaxies, namely, the supergalactic plane. The supergalactic plane is nearly perpendicular to the Galactic plane. If this structure is real then its existence places severe constraints on theories of cluster and supercluster formation. While Tully reports the detection at a "3 σ level," he did not rigorously estimate statistical significance of the structure. We will attempt to quantify this by asking how *often* would such large-scale anisotropy occur in a distribution with the observed small-scale clustering properties?

To answer this question, we have devised a statistical test that is both robust (insensitive to selection function) and sensitive to the presence of flattened distributions. We apply it to both the data and the simulations and determine the statistical significance of this flattening by computing the frequency of simulations that show larger anisotropies than the data.

We analyze the cluster distributions in the north and south Galactic hemispheres separately. Each hemisphere is divided into four different supergalactic latitude bins—each bin containing roughly the same number of clusters. For the purposes of this test we are only interested in the absolute value of the supergalactic latitude. We compare the redshift distributions of clusters in each supergalactic latitude bin. If there was a large flattened distribution of nearby clusters aligned with the supergalactic plane, there would be an abundance of clusters at low z (redshifts less than the maximum scale of the anisotropy) in the bin near the plane. Since the sample is supposedly bigger than the cluster complex, there should be no excess of clusters at high z (redshifts greater than the maximum scale of the anisotropy) in this same bin. Thus, the latitude bin near the plane would have more clusters at low z; the other latitude bins would have relatively more clusters at high z. The existence of substantial flattening will, therefore, manifest itself as a significant discrepancy between the redshift distributions in different latitude bins. We consider two distributions to be

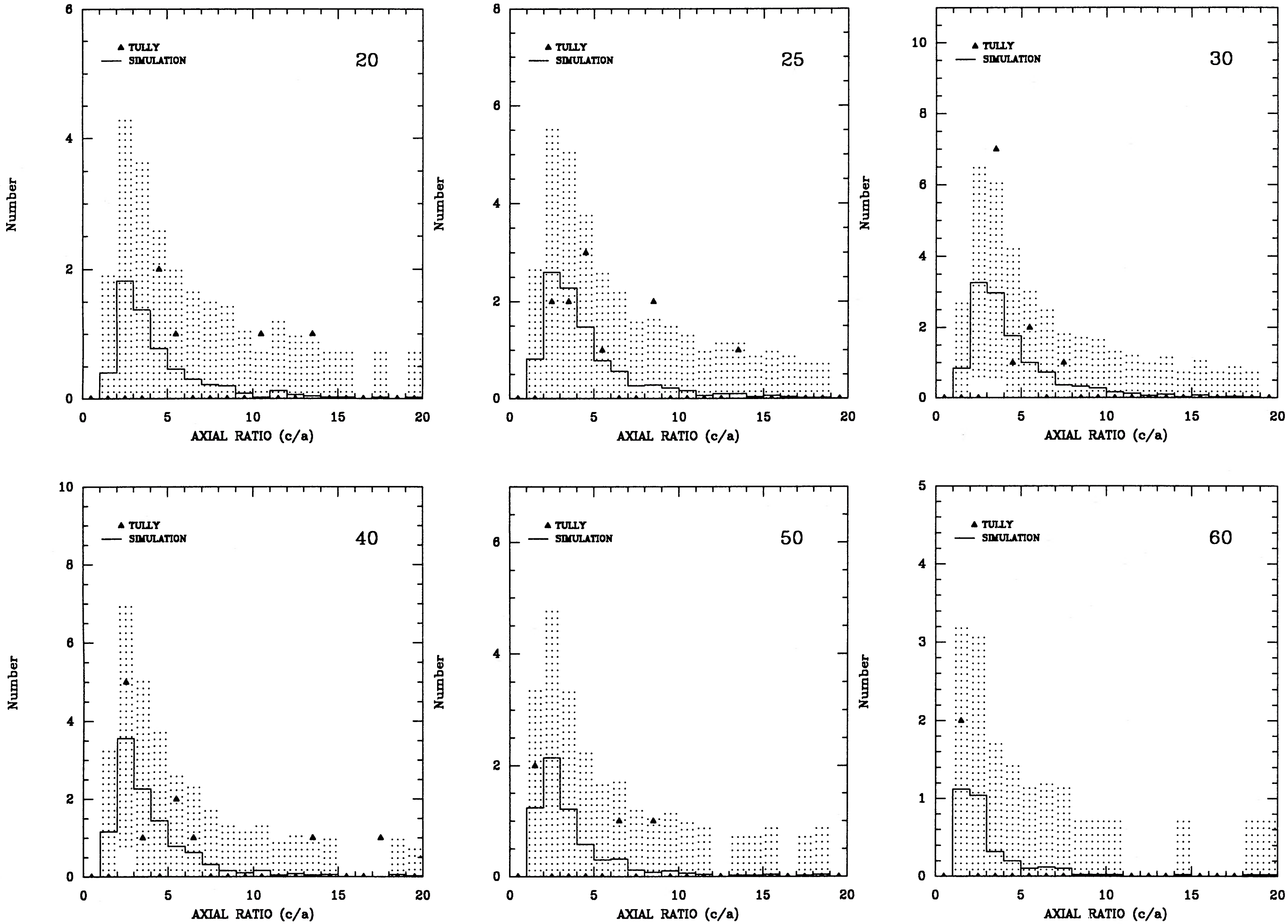

FIG. 5a

FIG. 5.—(*a*) Histograms of group axial ratios as a function of percolation length for the Tully sample and clustered simulations with correlation length $24h^{-1}$ Mpc. Triangles are the Tully cluster data. Solid histograms are the mean distributions for 50 realizations. Shaded areas are the 90% confidence limits on the mean histograms. The percolation length (in h^{-1} Mpc) is given in the upper right-hand corner of each histogram. (*b*) Histograms of group axial ratios as a function of percolation length for the Tully sample and a Poisson simulation set.

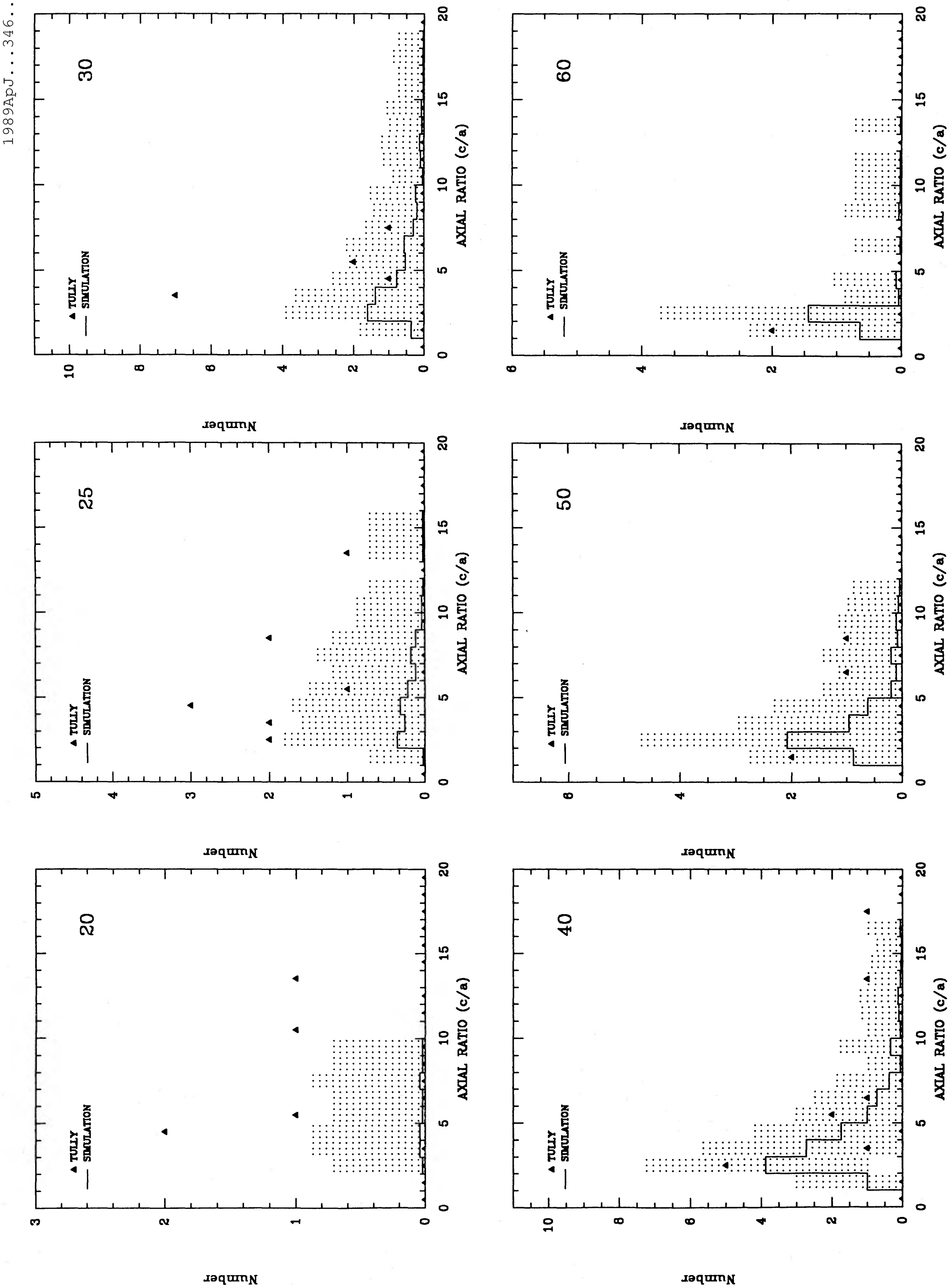

FIG. 5b

inconsistent if consistency is rejected at the 90% confidence level or greater by the Kolmogorov-Smirnov test.

This technique does not assume a specific form of the anisotropy but does require that the anisotropic structure be smaller than the depth of the sample. We tested the detection sensitivity of this technique by performing Monte Carlo simulations of 315 clusters. In these simulations, a fraction, f, of the clusters are distributed randomly in an oblate spheroid and the remainder are distributed randomly all over space. We are able to detect (at a $\gtrsim 90\%$ confidence level) the presence of an oblate spheroid with an axial ratio (x, y: z) of 1.5:1 with $f = 0.20$. The detection confidence level increases both with increasing axial ratio and increasing population fraction. For reference, the flattened supercluster complex reported in T87 has an axial ratio $\sim 2:1$ and $f \simeq 0.25$.

We first apply our technique to the real cluster samples. We find no significant flattening in Tully's northern sample of 201 Abell clusters, in agreement with Tully's own analysis. With four latitude bins, there are six independent pairs of latitude bins. None of the redshift distributions are significantly different from any other distribution. This result is confirmed by our analysis of the northern whole sky sample of 176 clusters. The two samples suggest different conclusions in the southern hemisphere. In the southern Tully sample of 114 clusters, two of the six possible comparisons of the four redshift distributions yield significant inconsistencies. In particular, clusters near the supergalactic plane have a significantly different redshift distribution than those far from the plane. In contrast, however, no inconsistencies are detected in the southern whole sky sample of 101 clusters. Although one usually expects the presence of structure to become more apparent as the sample size increases, the difference between the size of these two samples is small. The discrepancy between the two southern samples thus suggests that the significance of the detection in the Tully sample is, in fact, not high and that we probably need a larger cluster sample in order to make a more conclusive statement. We now turn to the simulations and ask how often are at least two out of the six pairs of latitude bins statistically different in at least one hemisphere?

We first analyze four sets of 50 Poisson simulations. The first set of simulations is generated with the magnitude limited redshift selection function and the H I+SW Galactic latitude selection function. The second set is generated with the magnitude-limited redshift selection function and the H I Galactic latitude selection function. The third set is generated with the magnitude-limited redshift selection function and the Abell galactic latitude selection function. The last set is generated with the full redshift selection function and the H I+SW galactic latitude selection function. The results in all four cases are nearly the same, namely, in only 6% of the simulations were two or more bin pairs discrepant at the 90% confidence level. The insensitivity of this result to the selection functions corroborates Tully's claim that the observed effect is not due to selection biases in redshift or Galactic latitude. The results also suggest that the observed flattening is a relatively rare occurrence—a "2 σ event"—arguing against the hypothesis that Abell clusters are drawn from a Poisson distribution.

In analyzing the clustered simulations, we also find that the frequency of significant anisotropy is independent of the Galactic latitude or redshift selection functions used (providing that extreme selection functions are excluded). We thus concentrate on measuring the dependence of the frequency of anisotropy on the cluster-cluster correlation length and on the value of the large-scale cutoff (corresponding to a small wavenumber cutoff in k-space). For this purpose we generate 19 sets of 50 clustered simulations, each set being generated with a different correlation length but all having the same correlation function slope of -1.8. The power spectra of all these simulations are cut off at small wavenumbers corresponding to spatial separations greater than $80h^{-1}$ Mpc. The magnitude-limited redshift selection function and the H I+SW Galactic latitude selection function were applied to the simulations. Figure 6 shows the flatness probability (the probability that a given simulation has a distribution at least as anisotropic as the southern Tully sample) as a function of the mean cluster-cluster correlation length for the 50 simulations in each set. There is a clear trend of increasing flatness probability as the correlation length increases. For correlation lengths $\gtrsim 20h^{-1}$ Mpc, the flatness probability is $\gtrsim 0.25$. The occurrence of deviations from isotropy like the kind seen in Tully's southern sample are thus not uncommon in clustered distributions ("1.2 σ events").

The dependence of flatness probability on the correlation length is probably a consequence of the fact that in a clustered distribution of 100–200 objects the number of statistically independent clumps is much less than the number of objects. Thus, the probability of chance alignments is higher—high enough, in fact, to cause significant anisotropy $\sim 25\%$–30% of the time in distributions with the observed two-point correlation function. Tully did propose this hypothesis as the only possible explanation that did not require the physical reality of the structure and, in fact, derived a flatness probability of 15%, not too different from our value. In light of the null detection in the whole sky survey, this hypothesis now seems reasonable.

Another relevant experiment is to measure the flatness probability as a function of the large-scale power cutoff. This will test whether or not such anisotropy requires power on very large scales. Figure 7 shows the flatness probability as a function of large-scale cutoff for 10 sets of 50 clustered simulations. Each set is generated with a different large-scale cutoff but all

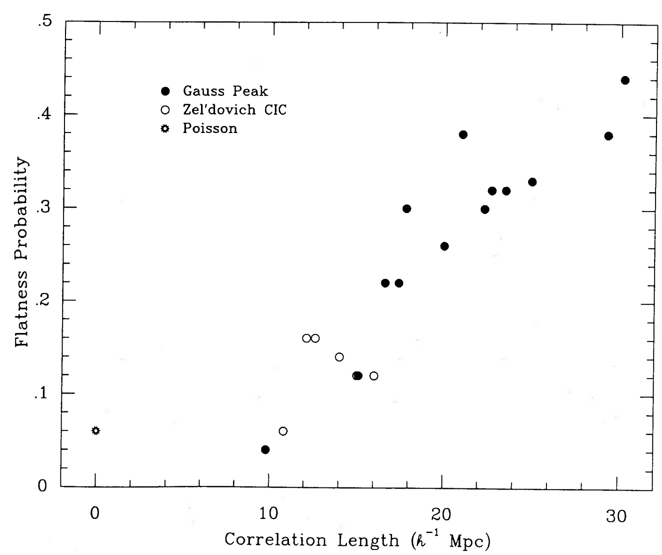

FIG. 6.—Flatness probability as a function of the cluster-cluster correlation length of the simulated catalog. Closed circles represent simulations generated by placing clusters at the peaks in a Gaussian density field. Open circles represent simulations generated using the Zel'dovich CIC algorithm. The starred datum is a representative Poisson simulation set.

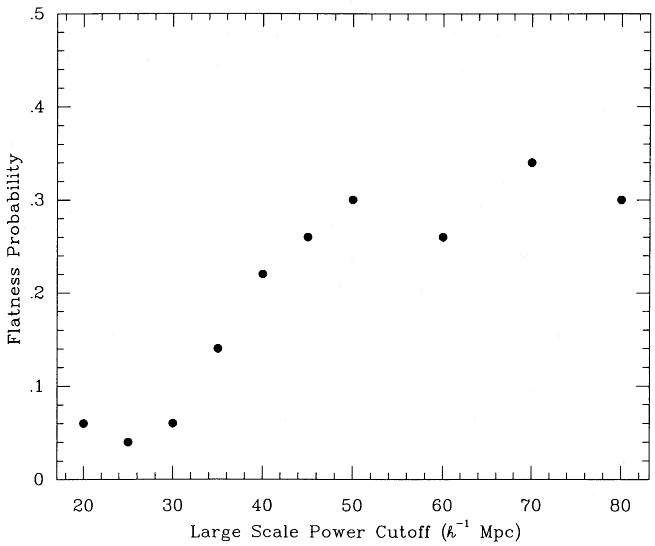

FIG. 7.—Flatness probability as a function of the large-scale power cutoff corresponding to a small wavenumber cutoff in the density perturbation power spectrum

have the same correlation length ($\sim 20h^{-1}$ Mpc), slope (-1.8), and selection biases. Figure 7 reveals that as long as the large-scale cutoff is greater than about $40h^{-1}$ Mpc, the flatness probability remains fairly constant at 0.25–0.35. The flatness probability begins to decline significantly only when the large-scale cutoff becomes less than $40h^{-1}$ Mpc. When the large-scale cutoff becomes comparable with the correlation length the flatness probability is consistent with results obtained for Poisson simulations. The anisotropy in the southern Tully sample appears, therefore, to be consistent with the superposition hypothesis and the presence of such features does not require power on scales greater than 40–$50h^{-1}$ Mpc.

VI. EFFECT ON HUBBLE FLOW AND THE MICROWAVE BACKGROUND

If complexes as massive as Tully claims do exist, they should leave measurable imprints on the microwave background. Here we will attempt to estimate the magnitude of such fluctuations. Following Tully (1986), we will assume that fluctuations in cluster counts equal fluctuations in mass, and $\delta N/N = \delta M/M \sim 1$ at $M \sim 10^{18}\ M_\odot$. We will make another crucial assumption, namely, that these clumps formed by gravitational instability from small initial random phase inhomogeneities. Under these two assumptions, we investigate how the presence of $10^{18}\ M_\odot$ clumps might perturb the Hubble flow and the brightness distribution of the cosmic microwave background radiation (CMB).

We find that the existence of such perturbations in an Einstein–de Sitter ($\Omega = 1$) universe would inevitably lead to excessive bulk motions on scales $\lesssim 50h^{-1}$ Mpc. The predicted streaming motions could be reconciled by lowering Ω. However, in low-Ω universes the bulk motions at the surface of last scattering will generate CMB anisotropy at levels which conflict with existing upper limits. In the $\Omega = 1$ universe these "primordial" bulk flows give rise to even larger anisotropy, also conflicting with recent measurements.

It is important to bear in mind that although the following calculations do not depend on the shape of the spectrum of primaeval density perturbations or the ionization history of the universe, they do depend on the two assumptions above. If supercluster complexes do not trace the mass and/or nongravitational forces are responsible for their formation then the conclusions of this section would not apply.

a) Bulk Flows at the Present Epoch

Linear perturbation theory predicts that the mean square bulk velocity, induced gravitationally on a comoving scale r by the inhomogeneous distribution of matter, is

$$\langle v^2 \rangle \equiv \sigma_V^2(r) = (Hf)^2 \int P(k)k^{-2} \exp(-k^2r^2)d^3k/(2\pi)^3 \ , \quad (4)$$

where P and k are the matter power spectrum and the comoving wavenumber, and we use Gaussian smoothing. In the linear regime, $f(\Omega) = \Omega^{0.6}$ (Peebles 1980). Equation (4) works remarkably well even in the mildly nonlinear regime, considered here (Villumsen and Davis 1986). The variance of mass fluctuations on scale R is

$$\langle (\delta M/M)^2 \rangle \equiv \sigma_M^2(R) = \int P(k) \exp(-k^2R^2)d^3k/(2\pi)^3 \quad (5)$$

and here we again use a Gaussian filter. Following Tully's conjecture, we will now assume

$$\sigma_M(50h^{-1}\ \text{Mpc}) = 1 \ . \quad (6a)$$

For comparison, note that galaxy counts on small scales ($hR < 10$ Mpc; Peebles 1980) give

$$\sigma_{\text{gal}}(R) \simeq 4\ \text{Mpc}/hR \ . \quad (6b)$$

A simple extrapolation of this law gives

$$\sigma_{\text{gal}}(50h^{-1}\ \text{Mpc}) \simeq 0.1 \ , \quad (6c)$$

an order of magnitude less than equation (6a). For an arbitrary power spectrum, the existence of mass fluctuations of given rms amplitude on scale R implies bulk flows on scales $r < R$, with

$$\sigma_V^2(r) \geq e(Hf)^2(R^2 - r^2)\sigma_M^2(R) \ , \quad (7)$$

(Juszkiewicz, Górski, and Silk 1987; Suto *et al.* 1988), where e is 2.718281828. The velocities have a Maxwellian distribution and therefore equation (6a) implies that, at a 95% confidence level, we can expect

$$v > 2800\Omega^{0.6}\ \text{km s}^{-1} \quad (8)$$

on scales $hr \ll 50$ Mpc. Unless $\Omega \leq 0.2$, this would be difficult to reconcile with $v \sim 600$ km s^{-1}, found for the Local Group's ($hr \sim 3$ Mpc) motion with respect to the CMB frame (Wilkinson 1988) and similar estimates for the bulk motion on much larger scales ($hr \sim 30$ Mpc; Faber and Burstein 1989, and Groth, Juszkiewicz, and Ostriker 1989).

b) Bulk Flows at the Surface of Last Scattering

The second set of constraints on the $\delta M/M$ field comes from upper bounds on the microwave radiation anisotropy. A clump of a comoving diameter of $2r$, located at the last scattering shell, subtends an angle

$$\theta \sim 1^\circ r_{50}\Omega \ , \quad (9)$$

where $r_{50} = hr/50$ Mpc. The residual CMB anisotropy on angular scales $< 2^\circ$ strongly depends on the ionization history of the universe. The smallest brightness fluctuations arise in models with full reionization of the hydrogen, occurring at redshifts $z > 20$. This is unlikely to happen in universes with adiabatic (constant entropy) initial perturbations and/or a dark nonbaryonic component. In these models fractional fluctuations in the CMB temperature, $\delta T/T$, are not attenuated by diffusion and, for a fixed value of $\delta M/M$, are larger than in universes with reheating. Thus a generic "minimal anisotropy" model (Kaiser 1984*a*), which allows reheating, is a baryon-dominated universe with spatial fluctuations in the initial distribution of entropy per baryon, like the family of fully ionized isocurvature models, recently considered by Peebles (1987). Below we will estimate minimal CMB anisotropy arising in such models with two different values of Ω and normalization set by equation (6a).

Density perturbations on scales smaller than the horizon, when matter and radiation have equal density [$k_*^{-1} = 5(\Omega h^2)^{-1}$ Mpc], generate $\delta T/T$ mainly through the Doppler effect (Sunyaev 1978), or Thomson scattering off bulk flows in the electron gas at the last scattering shell. On scales $r > k_*^{-1}$, the dominant sources of the anisotropy are gravitational potential wells around density fluctuations (the Sachs-Wolfe [1967] effect) and the isocurvature effect (Peebles 1987). In low-density models ($\Omega h < 0.1$), preferred because of the bound from the observed bulk flows (eq. [8]), the comoving scale of $50h^{-1}$ Mpc is smaller than k_*^{-1} and, hence, the CMB anisotropy is generated mainly through the Doppler effect.

To obtain a conservative estimate of $\delta T/T$, we assume that $P(k)$ has only one spectral line, with a wavenumber $k = h/50$ Mpc. The resulting correlation function for temperature fluctuations is

$$C(\theta) \equiv \langle \delta T(\theta)\delta T(0)\rangle T^{-2} = C(0)\sin(kx\theta)/(kx\theta) \quad (10a)$$

with $x = 2c/H\Omega$, where c is the velocity of light (Wilson and Silk 1981). The coherence angle for resulting brightness pattern is

$$\theta_c \equiv [-C(\theta)^{-1}d^2C(\theta)/d\theta^2]_{\theta=0}^{-1/2} \simeq 50\Omega r'_{50} . \quad (10b)$$

To estimate $C(0)$, we use the numerical results of Efstathiou and Bond (1987) who have integrated the Boltzmann transport equation for the cosmic background photons in universe models we consider here. Using equation (6a) to renormalize the results in their Figure 1*b*, we get rms temperature fluctuations

$$\sqrt{C(0)} = \begin{cases} 4 \times 10^{-4} & \text{for} \quad \Omega = 0.2 ; \\ 7 \times 10^{-4} & \text{for} \quad \Omega = 1 . \end{cases} \quad (11)$$

Both models assume isocurvature initial conditions and are fully ionized and baryon dominated; the Hubble parameter is $h = 0.5$. Our calculations have so far assumed a rather idealized "minimal" power spectrum. Any realistic $P(k)$ will obviously contain more than one spectral line. Since $\langle(\delta T/T)^2\rangle = C(0)$ is the sum of contributions from different wavenumbers, added in quadrature, it will be greater than our result which can be considered as a lower bound on $C(0)$, implied by equation (6a). The "realistic" value of θ_c may also be somewhat greater than our estimate. For fully ionized models, depending on Ω and the slope of the initial power spectrum, $n \equiv d \log P/d \log k$, θ_c varies from 20′ ($\Omega = 0.2$, $n = 0$) to 80′ ($\Omega = 1$, $n = -2$; Efstathiou and Bond 1987). Lowering n adds large-scale power and widens $C(\theta)$. Lowering Ω has the opposite effect due to the geometry of light propagation in negatively curved universes. In any case, it seems that if there are mildly nonlinear clumps with radii $\sim 50h^{-1}$ Mpc in the present epoch, we can safely expect CMB fluctuations with variance $C^{1/2}(0) > 10^{-4}$ and coherence angle $\theta_c \sim 1°\Omega$, for all "reasonable" cosmological parameters. For a Gaussian model of $C(\theta)$ recent experiments conducted at Caltech (Readhead *et al.* 1989) and Princeton (Timbie and Wilkinson 1989) give, respectively,

$$\sqrt{C(0)} < 10^{-4} \begin{cases} \text{for } 0\rlap{.}'5 < \theta_c < 15' \\ \text{for } \theta_c = 1\rlap{.}^\circ 1 . \end{cases} \quad (12)$$

Both limits satisfy the likelihood ratio test at the 95% confidence level. Clearly, the Caltech result is in conflict with the anisotropy that would be generated by all low-Ω universes with $\sigma_M(50h^{-1}\ \text{Mpc}) = 1$ while the Princeton result rules out the $\Omega = 1$ model.

VII. CONCLUSIONS

We performed an analysis of the statistical significance of the supercluster complexes reported in the Abell catalog by Tully. We generated two types of simulated catalogs, one based on the assumption that clusters are randomly distributed and the other based on the assumption that clusters are distributed with a two-point correlation function. After applying Galactic latitude and redshift selection effects to both samples, we use percolation to identify clusters in both the data and the simulated catalogs.

At percolation lengths less than $40h^{-1}$ Mpc, the frequency, density, and morphology of the observed Tully superclusters are reproduced well by the simulations with the known two-point correlation function. At larger percolation lengths, *both* the random and the clustered simulations produce complexes with similar frequency and properties as the Abell catalog. The presence of five supercluster "complexes" in the real data, in other words, is not unusual and does not require excess power on very large scales. They are merely the products of small-scale clustering and the behavior of percolation algorithms when run with percolation lengths that are comparable with the correlation length.

The 1 σ volume filling factor of superclusters as a function of percolation length in the real data agrees well with results from the clustered simulations for percolation lengths less than $40h^{-1}$ Mpc. Again, for larger percolation lengths, the volume filling factor of superclusters in the real data agrees well with results from *both* the random and clustered simulations. While clustered simulations with correlation lengths $\gtrsim 12h^{-1}$ Mpc match the observed dependence of the volume fraction on percolation length fairly well, the observed dependence of the population fraction on the percolation length is best reproduced by simulations with correlation lengths greater than $15h^{-1}$ Mpc. Simulations with correlation lengths greater than $30h^{-1}$ Mpc are inconsistent with the real data. For a given correlation length, there are no significant differences between simulations generated with the Zel'dovich CIC algorithm (where the cluster distribution is completely described statistically by the two-point correlation function) and simulations where clusters are placed at the peaks of a Gaussian random field (where higher order correlations are important).

The observed flattening of the southern cluster distribution in the supergalactic plane is not statistically significant. Inconsistency between the redshift distributions of clusters at different supergalactic latitudes was used to detect flattening. While flattening was seen in the Tully sample of 114 southern hemisphere clusters, this flattening was not confirmed by the slightly smaller (101 clusters) whole sky survey. To test that this apparent flattening is not due to Galactic extinction, simulations were run with no extinction, extinction derived from H I column densities, extinction derived from the Shane-Wirtanen counts, and extinction derived directly from counts of Abell clusters. In about 25%–35% of the clustered simulations, flattening comparable to that in the Tully sample was detected, independent of the redshift and Galactic latitude selection functions used. In constrast, such anisotropy is seen in only 6% of the Poisson simulations. We propose that the flattening is due to the chance superposition of a few superclusters. (Tully suggested this possibility and estimated its probability at 15%—he, however, emphasized the possibility that the large structures are real. We suspect that the structures are a manifestation of the small sample size—more data will resolve this question.) The superposition hypothesis is also supported by the independence of the flatness probability on the large-scale power cutoff when the cutoff is greater than $40h^{-1}$ Mpc.

The formation of massive ($10^{18}\ M_{\odot}$) supercluster complexes by gravitational instability about small initial random phase perturbations would have produced rms temperature fluctuations in the cosmic microwave background in excess of 10^{-4} on angular scales of $1°\Omega$. This can already be ruled out by current observations. The lack of large-scale microwave perturbations implies the nonexistence of $10^{18}\ M_{\odot}$ perturbations, a nongravitational origin to supercluster complexes, or a fundamental flaw in our standard cosmology. Peculiar velocities of the clusters in these complexes would be $\gtrsim 2800\Omega^{0.6}$ km s^{-1}, a value that, for a high-density universe, conflicts with several studies of the deviations from Hubble flow by rich clusters (Rood 1976; Wagner and Perrenod 1981; Bahcall, Soneira, and Burgett 1986; Postman, Geller, and Huchra 1988; Soltan 1988; Faber and Burstein 1989).

In conclusion, we can reject the null hypothesis that the Abell clusters are drawn from a random sample. Tully's reported structures are real in the sense that they contradict this hypothesis. However, previous studies have demonstrated the existence of two-point correlations between clusters. The present data do not require correlations beyond $45h^{-1}$ Mpc. There is not (yet) any definitive evidence for structure on the scale of $300h^{-1}$ Mpc.

We thank Brent Tully, Adrian Melott, and Jeremiah Ostriker for their insightful comments and the referee, Steve Shectman, for his careful reading of the manuscript. The authors also wish to thank the Aspen Center for Physics where some of this work was done. Summary results from this study were presented at the Topology Workshop at the University of Kansas, Lawrence, Kansas, 1988 April. M. Postman acknowledges support from NSF grant AST86-18257. D. Spergel was supported, in part, by NSF grants PHY88-05895, AST88-58145, and a Sloan Foundation fellowship. R. Juszkiewicz thanks Dave Wilkinson for his hospitality at the Princeton University Physics Department and John Bahcall at the Institute for Advanced Study. R. Juszkiewicz was supported in part, by New Jersey High Technology grant 88-240090-2.

REFERENCES

Abell, G. O. 1958, *Ap. J. Suppl.*, **3**, 211.
Bahcall, N. A. and Soneira, R. M. 1983, *Ap. J.*, **270**, 20.
Bahcall, N. A., Soneira, R. M., and Burgett, W. S. 1986, *Ap. J.*, **311**, 15.
Burstein, D., and Heiles, C. 1978, *Ap. J.*, **225**, 40.
Efstathiou, G., and Bond, R. 1987, *M.N.R.A.S.*, **227**, 33P.
Efstathiou, G., Davis, M., Frenk, C. S., and White, S. D. M. 1985, *Ap. J. Suppl.*, **54**, 241.
Faber, S. M., and Burstein, D. 1989, in *Large Scale Motions in the Universe*, ed. G. Cogue and V. C. Rubin (Vatican City: Pontificial Academy of Sciences), in press.
Fisher, J. R., and Tully, R. B. 1981, *Ap. J. Suppl.*, **47**, 139.
Groth, E. J., Juszkiewicz, R., and Ostriker, J. P. 1989, *Ap. J.*, **346**, 558.
Heiles, C. 1975, *Astr. Ap. Suppl.*, **20**, 37.
Huchra, J. P., Geller, M. J., and Postman, M. 1989, in preparation.
Huchra, J. P., Henry, J. P., Postman, M., and Geller, M. J. 1989, in preparation.
Juszkiewicz, R., Górski, K., and Silk, J. 1987, *Ap. J. (Letters)*, **323**, L1.
Kaiser, N. 1984*a*, *Ap. J.*, **282**, 374.
———. 1984*b*, *Ap. J. (Letters)*, **284**, L9.
Klypin, A., and Kopylov, A. 1983, *Soviet. Astr. Letters*, **9**, 41.
Mattig, W. 1958, *Astr. Nach.*, **284**, 109.
Peebles, P. J. E. 1980, *Large Scale Structure in the Universe* (Princeton: Princeton University Press), p. 63.
———. 1987, *Ap. J. (Letters)*, **277**, L1.
Postman, M., Geller, M. J., and Huchra, J. P. 1986, *A.J.*, **91**, 1267.
———. 1988, *A.J.*, **95**, 267.
Readhead, A. C. S., Lawrence, C., Myers, S. T., and Sargent, W. L. W. 1989, *Ap. J.*, **346**, 566.
Rood, H. J. 1976, *Ap. J.*, **207**, 16.
Sachs, R. K., and Wolfe, A. M. 1967, *Ap. J.*, **147**, 73.
Shane, C. D., and Wirtanen, C. A. 1967, *Pub. Lick Obs.*, **22**, 1.
Shectman, S. A. 1985, *Ap. J. Suppl.*, **57**, 77.
Soltan, A. 1988, *M.N.R.A.S.*, **231**, 309.
Sunyaev, R. 1978, in *IAU Symposium 79, Large Scale Structure in the Universe*, ed. M. S. Longair and J. Einasto (Dordrecht: Reidel), p. 393.
Sutherland, W. 1988, *M.N.R.A.S.*, **234**, 159.
Suto, Y., Gòrski, K., Juszkiewicz, R., and Silk, J. 1988, *Nature*, **332**, 328.
Timbie, P. T., and Wilkinson, D. T. 1989, *Ap. J.*, in press.
Tully, R. B. 1986, *Ap. J.*, **303**, 25.
———. 1987, *Ap. J.*, **323**, 1 (T87).
Villumsen, J., and Davis, M. 1986, *Ap. J.*, **308**, 499.
Wilkinson, D. T. 1988, in *IAU Symposium 104, Early Evolution of the Universe and its Present Structure*, ed. J. Audouze and A. S. Szalay (Dordrecht: Reidel), p. 143.
Wilson, M. L., and Silk, J. 1981, *Ap. J.*, **243**, 14.
Wagner, R. M., and Perrenod, S. C. 1981, *Ap. J.*, **251**, 424.

ROMAN JUSZKIEWICZ: Institute for Advanced Study, Olden Lane, Building E, Princeton, NJ 08540

MARC POSTMAN and DAVID N. SPERGEL: Department of Astrophysical Sciences, Peyton Hall, Princeton University, Princeton, NJ 08544-1001

BRIAN SUTIN: Astronomy Program, University of Maryland, College Park, MD 20742